Design and CFD Analysis of Wickless Heat Pipes Filled with Refrigerants as Working Fluids for HVAC Applications

B. Sivaramakrishnan and J. Selwin Rajadurai

Abstract Heat pipes are heat transfer devices with very good thermal conductivity. Heat pipes with refrigerants as working fluids were investigated. The refrigerants used in this work are R134a and R404a. Gravity-assisted heat pipe was preferred to this application. The various heat transfer limits in the design of heat pipes were found. The thermal performance of the heat pipes was studied by computational fluid dynamics method. ANSYS Fluent 16.0 was used to perform the CFD analysis. VOF method was employed. Very low heat input was applied for this particular application. The temperature distribution along the length of the heat pipe was studied. The CFD results are validated with the experimental values of the reference work. The thermal resistance values are found and compared with the experimental work. Optimization was performed using Taguchi technique.

Keywords Heat pipes · Refrigerants · Computational fluid dynamics · ANSYS Fluent

List of Symbols

Q_{sonic}	Sonic limit
Q_{viscous}	Viscous limit
$Q_{\text{entrainment}}$	Entrainment limit
Q_{boiling}	Boiling limit
A_{v}	Area of the vapor space
L	Latent heat of evaporation

B. Sivaramakrishnan (✉)
Engineering Design, Department of Mechanical Engineering,
Government College of Engineering, Tirunelveli 627007, India
e-mail: sivarama1196@gmail.com

J. Selwin Rajadurai
Department of Mechanical Engineering, Government College of Engineering,
Tirunelveli 627007, India

L.-J. Yang et al. (eds.), *Proceedings of ICDMC 2019*,
Lecture Notes in Mechanical Engineering,
https://doi.org/10.1007/978-981-15-3631-1_57

ρ_v	Density of the vapor phase
ρ_l	Density of the liquid phase
P_v	Vapor pressure
D_i	Inner diameter of the thermosyphon
r_v	Radius of the vapor space
l_{eff}	Effective length of the heat pipe
l_{ad}	Length of the adiabatic section
l_c	Length of the condenser section
μ_v	Viscosity of the vapor phase
f_1, f_2, f_3	Entrainment factors
g	Acceleration due to gravity
σ_l	Surface tension of the liquid phase
B_0	Bond number
Q	Heat input
T_e	Temperature of the evaporator section
T_c	Temperature of the condenser section
R	Thermal resistance
Seq SS	Sequential sum of squares
Adj SS	Adjusted sum of squares
DF	Degree of freedom
Adj MS	Adjusted mean squares
CFD	Computational fluid dynamics

1 Introduction

Heat pipes are efficient heat transfer devices with very less thermal resistance. Heat pipes are used in heating, ventilation and air-conditioning, electronic circuits, electric motors, air preheating, IC engines, heat exchangers, aerospace, satellites and human body temperature control.

Experimental investigation of the performance of two-phase closed thermosyphon filled with refrigerants R134a, R404a and R407C was reported [1]. The performance of R407C was 50% lower than other two. Thermal performance analysis of nanofluids in a thermosyphon heat pipe using computational fluid dynamics was done. De-ionized water and CuO/water nanofluid were used as working fluids [2]. Rahimi et al. [3] in their experiment reported the performance of thermosyphon at different operating conditions. The experimental measurements were compared with the predicted CFD temperature, and a good agreement was observed. Sozen et al. [4] made an investigation to utilize the Fly ash nanofluids in a two-phase closed thermosyphon for enhancing the heat transfer. The nanofluid filled 33.3% of the volume of the two-phase closed thermosyphon. Three heating power levels (200, 300 and 400 W) were used in the experiments with three different cooling water flow rates. Vafai et al. [5] utilized analytical models to investigate the thermal performance of rectangular-

and disk-shaped heat pipes using nanofluids. Al_2O_3, CuO and TiO_2 with a range of diameters are utilized to form the nanofluid. Khandekar et al. [6] used distilled water and acetone as the working fluid. Experimental investigation of a thermosyphon-based heat exchanger used in energy-efficient air handling units was done [7]. Nine thermosyphons in a modified inline configuration filled with water as working fluid were used. The experimental setup has finned evaporator and condenser sections. The overall effectiveness and thermal resistance of the heat pipe heat exchanger were found. Thermal analysis of heat pipe using Taguchi technique was done. Heat input (W), angle of inclination (deg) and flow rate (kg/min) were taken as the parameters. Efficiency, thermal resistance and overall heat transfer coefficient were found. *L*9 orthogonal array was used [8]. Narayan et al. [9] developed flexible heat pipes. With the straight and bend configurations of the heat pipe, the thermal resistance is reported. This flexibility will prevent damage to the heat pipe against the vibratory motion. Panda et al. [10] developed high-temperature heat pipes and thermosyphons for compact high-temperature reactor. CFD analysis was done. A three-dimensional transient numerical model has been developed to predict the vapor core, wall temperatures, vapor pressure and vapor velocity in the screen mesh wick. Huminic et al. [11] investigated the heat pipes with water–nanoparticle mixtures. Water is used as a base working fluid. Copper oxide was used as the nanoparticles. Volume fraction of 0, 1 and 4% for CuO is considered the analysis. Deshpande et al. [12] theoretically designed radiators using heat pipes. Design calculations for heat pipe were performed. The maximum heat transfer limit was $Q_{max} = 405.7$ W. Effect on dimensions of the radiator and effect on heat capacity were discussed. As the capacity of the radiator is reduced, the exit temperature of the water is increased. Investigation of the thermal performance of two-phase closed thermosyphon charged with R134a and R404a were done. CFD modeling was done [13].

El-Sharkawy [14] evaluated the performance of heat pipe heat exchanger for automotive applications. Design of experiments was performed. Eight control factors and three levels were taken. Heat pipe design software tool was used to investigate the thermal performance of the heat exchanger design for automotive applications. Umberto Costa Bitencourt [15] explains the CFD procedure for the simulation of pulsating heat pipe. Bhanu Prakash et al. [16] performed thermal analysis of heat pipe with inclined 60° and 90° orientation. Acetone was used as the working fluid. Girish et al. [17] done CFD analysis in the pulsating heat pipe. Pandiraj et al. [18] used MgO nanofluids for thermal performance enhancement in flat plate heat pipes.

Very few CFD works were carried out for heat pipes with refrigerants as working fluids. In this work, theoretical thermal design calculations were performed. Heat pipes with different fill ratios were investigated.

2 Design of Heat Pipes

Design of heat pipes involves the theoretical determination of heat transfer limits using the correlations [12] (Fig. 1; Table 1).

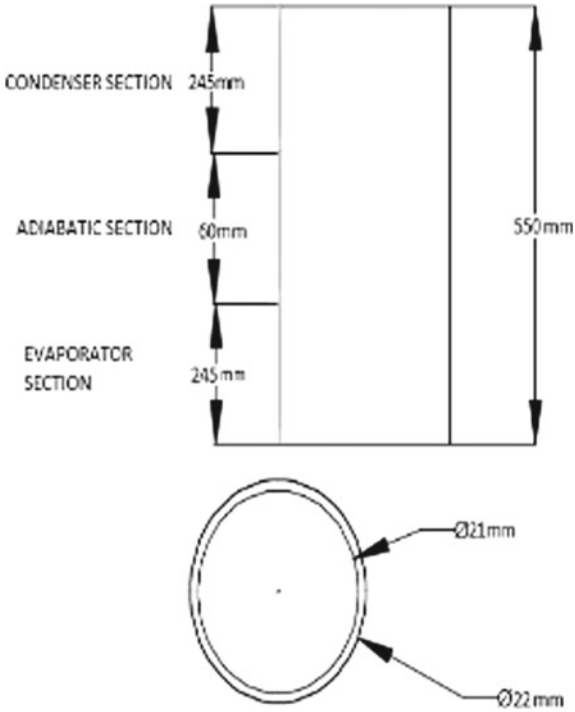

Fig. 1 Geometry of the heat pipe

Table 1 Specifications of the heat pipe [1]

Length of the evaporator section (mm)	245
Length of the adiabatic section (mm)	60
Length of the condenser section (mm)	245
Outer diameter of the thermosyphon (mm)	22
Inner diameter of the thermosyphon (mm)	20
Working fluids	R134a, R404a

2.1 Sonic Limit

As the temperature of the vapor in the heat pipe is lowered, the vapor pressure drops. The vapor velocity must increase to carry a given amount of heat, which in turn increases the pressure drop from the evaporator to the condenser. Compressible flow effects become important at these low vapor pressures.

$$Q_{\text{sonic}} = 0.474 \times A_{\text{v}} \times L \times (\rho_{\text{v}} \times P_{\text{v}})^{0.5}$$

where $A_{\text{v}} = \frac{\pi}{4} D_{\text{i}}^2$.

2.2 Viscous Limit

The saturation vapor pressure is of the same magnitude as the pressure drop required to drive the vapor flow. There is an insufficient pressure available to drive the vapor. The viscous limit occurs at low operating temperature.

$$Q_{\text{viscous}} = \frac{A_\text{v} \times r_\text{v} \times L \times \rho_\text{v} \times P_\text{v}}{16 \times \mu_\text{v} \times l_\text{eff}}$$

2.3 Entrainment Limit

Dry out of the evaporator section may occur. This limit refers to the case of high shear forces developed as the vapor passes in the counterflow direction over the liquid-saturated wick, where the liquid may be entrained by the vapor and returned to the condenser.

$$Q_{\text{entrainment}} = A_\text{v} \times L \times f_1 \times f_2 \times f_3 \times \rho_\text{v}^{0.5} \times (g \times \sigma_\text{l} \times (\rho_\text{l} - \rho_\text{v}))^{0.25}$$

f_1 is a function of bond number (Figs. 2 and 3)

Bond Number, $B_\text{o} = D_\text{i} \times \left(\frac{g \times \rho_\text{l} - \rho_\text{v}}{\sigma_\text{l}}\right)^{0.5}$

f_2 is a function of dimensionless parameter

$$K_\text{p} = \frac{P_\text{v}}{(g \times (\rho_\text{l} \times \rho_\text{v})^{0.25})}$$

$f_3 = 1$ (since the thermosyphon is vertical).

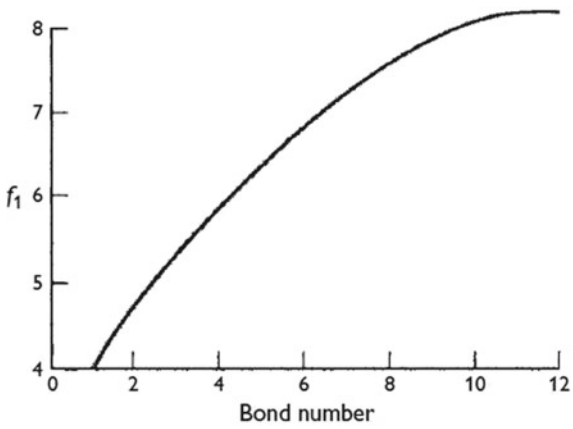

Fig. 2 Effect of bond number versus entrainment factor f_1 [14]

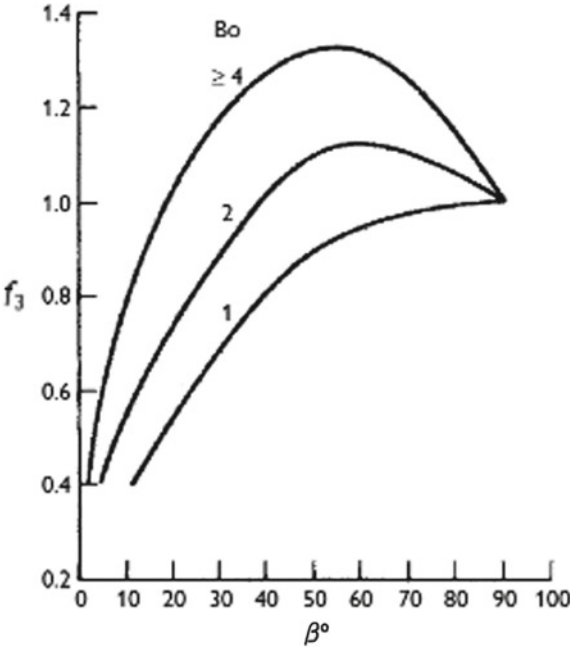

Fig. 3 Inclination angle versus entrainment factor f_3 [14]

2.4 Boiling Limit

The boiling limit occurs when the applied evaporator heat flux is sufficient to cause the nucleate boiling in the evaporator. This creates vapor bubbles that partially block the liquid return and can lead to evaporator dryout. Heat flux limit is the other name for boiling limit (Tables 2, 3 and 4).

Table 2 Properties of the working fluids

Properties/working fluids	R134a	R404a
Latent heat of evaporation (kJ/kg)	177.79	140.25
Density of vapor phase (kg/m^3)	32.35	1044.2
Density of liquid phase (kg/m^3)	1207.6	65.247
Specific heat of liquid phase (kJ/kg K)	1.4246	1.5423
Specific heat of vapor phase (kJ/kg K)	1.0316	1.2214
Thermal conductivity of liquid phase (W/m K)	0.081134	0.063625
Thermal conductivity of vapor phase (W/m K)	0.013825	0.015905
Viscosity of liquid phase (kg/m s)	1.9489×10^{-4}	1.2827×10^{-4}
Viscosity of vapor phase (kg/m s)	1.1693×10^{-5}	1.2152×10^{-5}
Molecular weight (kg/k mol)	102.03	97.604

Table 3 Properties of container material (copper)

Density of copper (kg/m^3)	8960
Specific heat (J/kg K)	376.812
Thermal conductivity (W/m k)	401

Table 4 Heat transfer limits

Working fluid	Sonic limit (W)	Viscous limit (W)	Entrainment limit (W)	Boiling limit (W)
R134A	122.72×10^{-3}	210.46	2.05×10^{-3}	118.9
R404A	122.47×10^{-3}	264.7	450.9	158.91

$$Q_{\text{boiling}} = 0.12 \times A_{\text{v}} \times L \times \rho_{\text{v}}^{0.5} \times ((g \times \sigma_{\text{l}} \times (\rho_{\text{l}} - \rho_{\text{v}}))^{0.25})$$

Thermal design calculations were performed. Various heat transfer limits in the design of heat pipes were found and are tabulated.

3 CFD Analysis

The two-dimensional models were created by using the line command, and the surfaces are created using the surface from sketch command in the ANSYS design modeler. The fine mesh was applied. There are 3324 nodes and 3036 elements after meshing. The elements are quadrilateral elements. In the general tab, the transient model was chosen. Because there is a dependence on time and there is no steady-state operation. The gravity was set as 9.81 m/s^2 in the negative y-direction. The multiphase model was clicked twice, and the properties were set. The three Eulerian phases are air, R134a liquid and R134a vapor. The reason for including a phase with air is that if only water liquid and vapor are defined as the phases, the calculation starts as water vapor is already present inside the pipe [15].

The implicit body force box was checked. The energy equation was turned on to allow heat transfer between the phases and the flow is K-ϵ model. The models used in the analysis are the multiphase model and viscous model. The number of mass transfer mechanism is 1. The evaporation and condensation frequency is set as 0.1. The saturation temperature is enabled as 297.69 K. Implicit first-order upwind scheme was used for solving the governing equation. The VOF model is used for analysis. The turbulence model applied for the present analysis was the Reynolds stress model. The SIMPLE scheme was selected. The first-order upwind momentum was checked. To solve the Navier–Stoke equation, the widely used numerical procedure was the SIMPLE algorithm. SIMPLE means for semi-implicit method for pressure-linked equations. The time step size is 0.0005. The number of time steps is 100. Maximum iterations per time step were given as 10.

3.1 Volume of Fluid Method

The volume of fluid method was used in this analysis. It is a numerical method of free surface approximations. It is classified as the Euler method. A good method for volume tracking and locating the free surface is the volume of fluid method. With the most suitable jump boundary conditions at the interface, the motion of different phases is solved by a single set of transport equations. Two or more immiscible fluids can be solved by a single set of momentum equations in the VOF model. There are two conditions when a steady-state VOF calculation is practical. They are (i) the inflow boundary conditions of the individual phases are distinct and (ii) the solution is independent of the initial conditions.

The fill ratio is defined as the ratio of the volume filled by the working fluid to the total volume of the heat pipe.

4 Results and Discussions

Figure 4 shows the temperature distribution along the length of the heat pipe. It was clearly identified that the temperature in the evaporator section (306–301 K) is more than the condenser and adiabatic section. This is due to the fact that the heat is supplied at the evaporator section. In the adiabatic section, there is only some heat loss to the surrounding. In the condenser section, the temperature varies from 295 to 291 K. From the plot, it is clear that the working fluid inside the heat pipe evaporates in the evaporator section and condenses in the condenser section. And the condensate returns back to the evaporator by means of gravity. Since the heat pipes were gravity assisted, there is no need of wick structure inside the heat pipe. Figure 5 shows the liquid volume fraction contours of the heat pipe filled with R134A as working fluids.

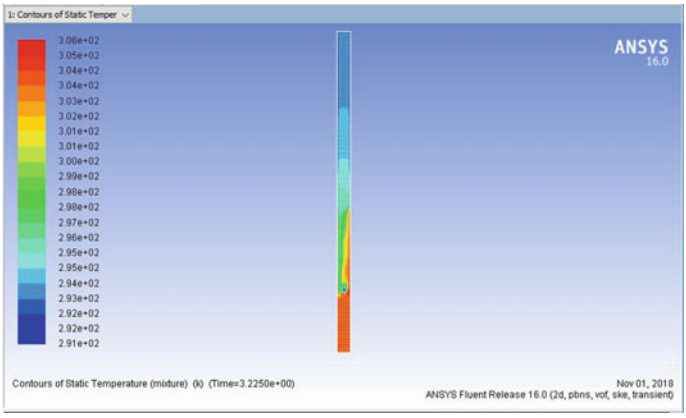

Fig. 4 Temperature distribution of heat pipe with R134A as working fluid with 30% fill ratio

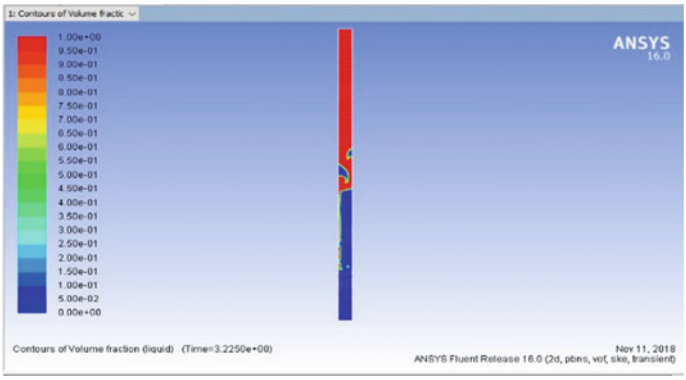

Fig. 5 Volume fraction contours of the heat pipe filled with R134a

The volume fraction contour confirms the process of nucleate pool boiling inside the heat pipe.

The temperature distribution in the heat pipe using R404a is shown in Fig. 6. The temperature distribution in the evaporator section varies from 303 to 300.5 K (Fig. 7). The temperature is maintained constant in the adiabatic section. The temperature varies from 296 to 294 K in the adiabatic section. The plot shows very clearly the working fluid in the heat pipe evaporates at the evaporator section and condenses at the condenser section and also indicates the condensate return across the boundary which is blue in color.

Thermocouple locations from 1 to 3 are in the evaporator section. Adiabatic section has two thermocouples (4 and 5). Thermocouples 6, 7 and 8 are located in the condenser section. The figure shows that there is only little deviation from the experimental and CFD value. And the temperatures found by CFD analysis were

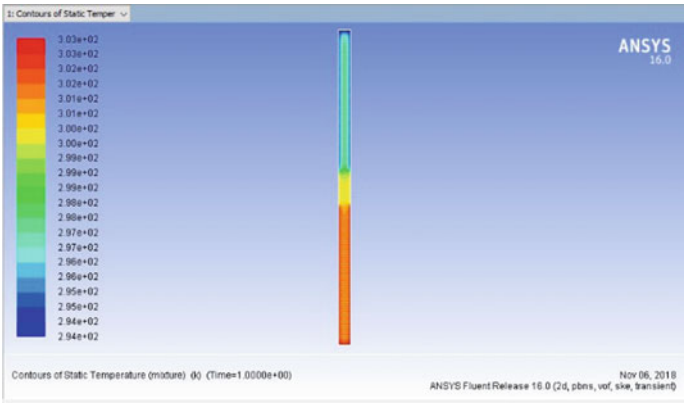

Fig. 6 Temperature distribution of the heat pipe with R404a as working fluid 30% fill ratio

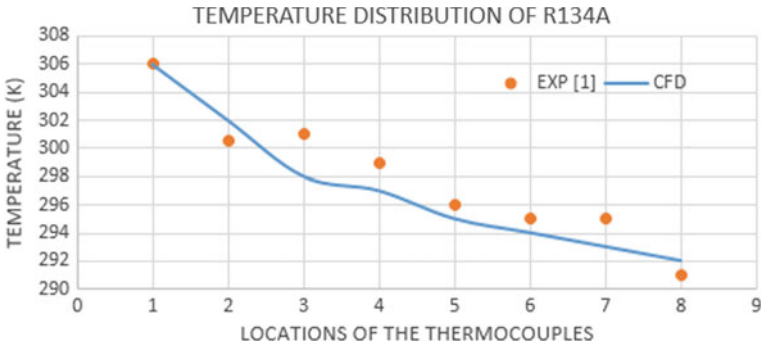

Fig. 7 Temperature distribution with R134a as working fluid along the length of the heat pipe

found to be in agreement with the experimental values. The values obtained from the CFD analysis are validated with the experimental results. The temperature in the evaporator section is more due to the supply of heat. The heat loss takes place at the condenser section. The CFD values are found to be in agreement with the experimental values (Fig. 8).

Figure 9 shows the comparison between the heat pipes with R134a and R404a as the working fluids. For the same heat input, the performance of R134A is almost equal to the thermal performance of the heat pipe with R404a as working fluid. The formula for calculating the thermal resistance is given below (Figs. 10, 11, 12, 13 and 14; Tables 5 and 6):

$$R = \frac{T_e - T_c}{Q} \text{ K/W}$$

The reason for selecting the fill ratios in increasing order from 10, 20, 30, 40 and 50% is to ensure the evaporation and condensation inside the heat pipe.

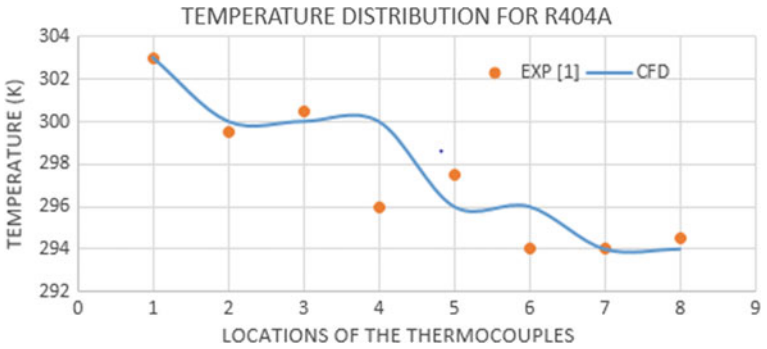

Fig. 8 Temperature distribution of heat pipe with R404a as working fluid with 30% fill ratio

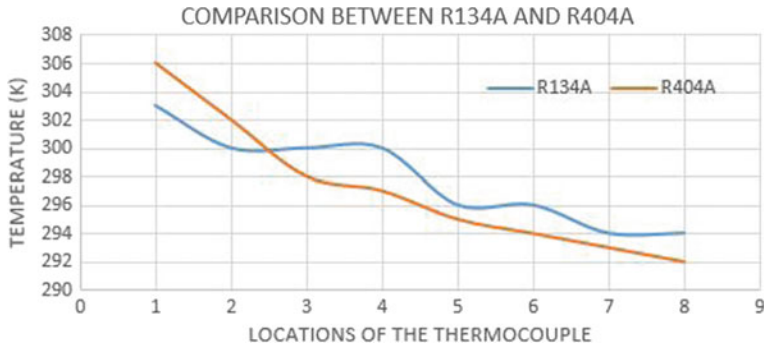

Fig. 9 Temperature distribution of heat pipe with R134A and R404A

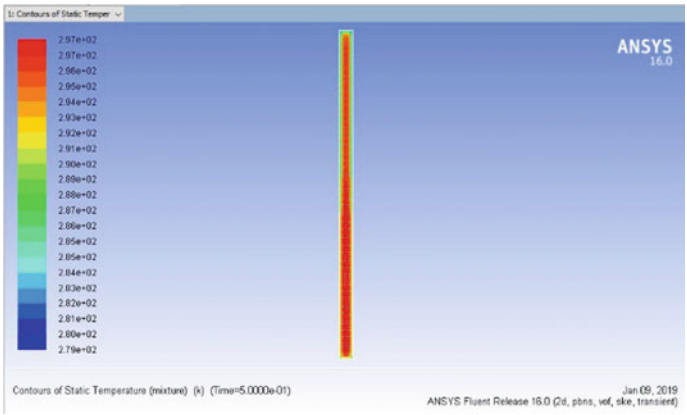

Fig. 10 Temperature distribution of heat pipe with R404a as working fluid with 10% fill ratio

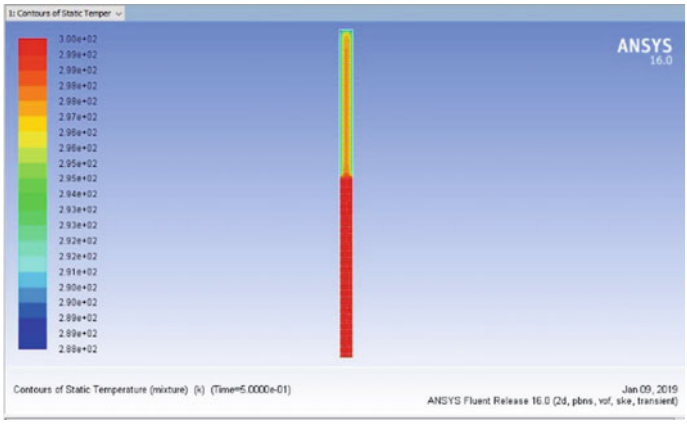

Fig. 11 Temperature distribution of heat pipe with R404a as working fluid with 20% fill ratio

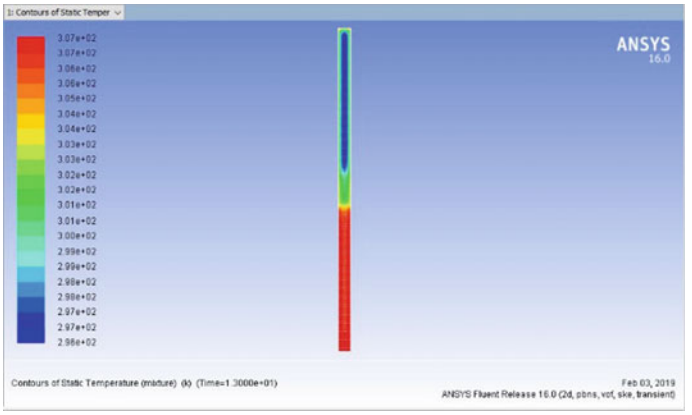

Fig. 12 Temperature distribution of heat pipe with R404a as working fluid with 40% fill ratio

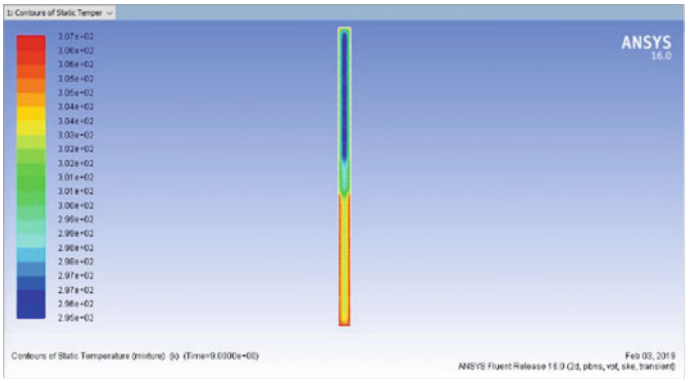

Fig. 13 Temperature distribution of heat pipe with R404a as working fluid with 50% fill ratio

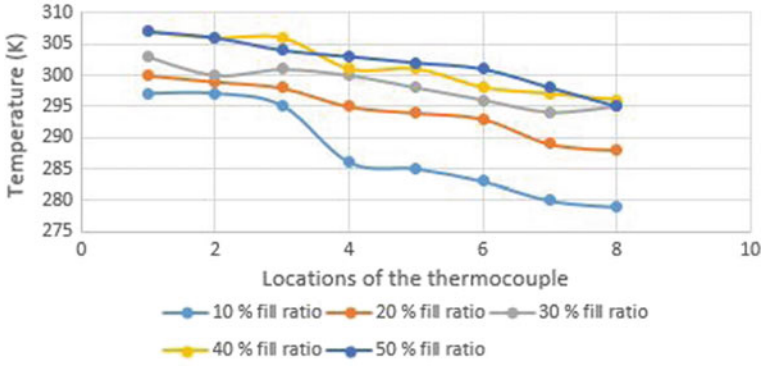

Fig. 14 Temperature distribution of heat pipes with R404a as working fluid with different fill ratios

Table 5 Comparison between CFD and experimental value [1]

S. No.	Working fluid	Thermal resistance experimental value[a] (K/W)	Thermal resistance CFD value (K/W)	Error (%)
1	R134A	0.375	0.35	6.67
2	R404A	0.2125	0.2	5.88

[a]The experimental thermal resistance values are calculated from the temperature distribution plot of the Grezgorz Gorecki [1]

Table 6 Fill ratio and thermal resistance

Fill ratio (%)	Thermal resistance (K/W)
10	0.45
20	0.30
30	0.225
40	0.275
50	0.3

Effect of fill ratio on thermal resistance

The value of the thermal resistance increases with increase in fill ratio up to 40%, and it suddenly decreases at 50% fill ratio.

5 Optimization Using Taguchi Technique

The number of levels taken for this analysis was five and the control parameters were two. Therefore, the *L*25 orthogonal array was selected. Twenty-five runs were conducted with R404a as working fluid. This is because the thermal resistance value is low compared to R134a (Table 7).

5.1 Orthogonal Array for L*25 Design*

See Table 8.

Table 7 Control parameters and number of levels

Control parameters	Level 1	Level 2	Level 3	Level 4	Level 5
Heat input (W)	10	20	30	40	50
Fill ratio (%)	10	20	30	40	50

Table 8 *L*25 design

*L*25	Level 1	Level 2
1	1	1
2	1	2
3	1	3
4	1	4
5	1	5
6	2	1
7	2	2
8	2	3
9	2	4
10	2	5
11	3	1
12	3	2
13	3	3
14	3	4
15	3	5
16	4	1
17	4	2
18	4	3
19	4	4
20	4	5
21	5	1
22	5	2
23	5	3
24	5	4
25	5	5

The formula for calculating S/N ratio is $-10\log\left[\frac{1}{y_i^2}\right]$ (Table 9).

Taguchi analysis: Thermal resistance (K/W) versus heat input (W) and fill ratio (%) response table for signal-to-noise ratios.

Smaller is better (Fig. 15; Table 10).

Taguchi analysis: Heat transfer coefficient (W/m^2 K) versus heat input fill ratio (%) response table for signal-to-noise ratios.

Larger is better (Fig. 16; Table 11).

Table 9 S/N ratios for thermal resistance and heat transfer coefficient

Heat input (W)	Fill ratio (%)	Thermal resistance (K/W)	Heat transfer coefficient (W/m^2K)	S/N ratio 1	S/N ratio 2
10	10	1.3	83.32	−2.27887	38.41499
10	20	0.9	120.35	0.91515	41.60892
10	30	0.8	135.4	1.9382	42.63237
10	40	0.9	120.359	0.91515	41.60957
10	50	1	108.3235	0	40.69445
20	10	0.75	144.43	2.498775	43.19315
20	20	0.6	180.53	4.436975	45.13099
20	30	0.4	270.8	7.9588	48.65297
20	40	0.5	216.64	6.0206	46.71477
20	50	0.65	166.64	3.741733	44.43559
30	10	0.67	162.49	3.478504	44.21653
30	20	0.43	249.98	0.43	47.95811
30	30	0.3	361.07	0.3	51.15183
30	40	0.36	295.43	0.36	49.40909
30	50	0.4	270.81	0.4	48.65329
40	10	0.45	240.72	0.45	47.63024
40	20	0.3	361.08	0.3	51.15207
40	30	0.225	481.44	0.225	53.65084
40	40	0.275	393.404	0.275	51.89678
40	50	0.3	361.08	0.3	51.15207
50	10	0.44	246.19	0.44	47.82541
50	20	0.28	386.87	0.28	51.7513
50	30	0.24	451.3457	0.24	53.09019
50	40	0.3	361.07	0.3	51.15183
50	50	0.34	318.6	0.34	50.06492

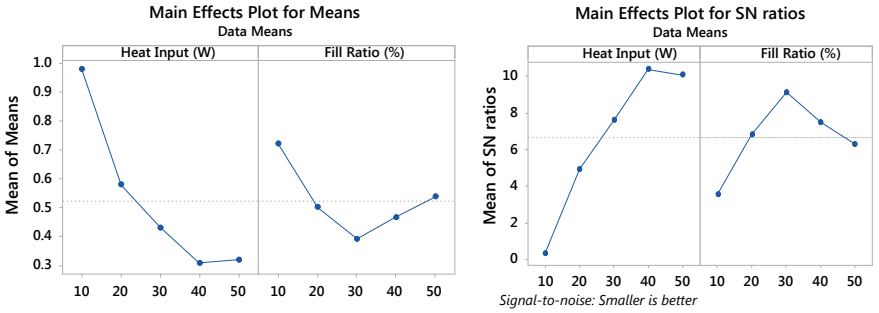

Fig. 15 Effect on thermal resistance

Table 10 Response table for thermal resistance

Level	Heat input (W)	Fill ratio (%)
1	0.2979	3.5530
2	4.9314	6.8394
3	7.6199	9.1413
4	10.4041	7.4961
5	10.0823	6.3057
Delta	10.1062	5.5883
Rank	1	2

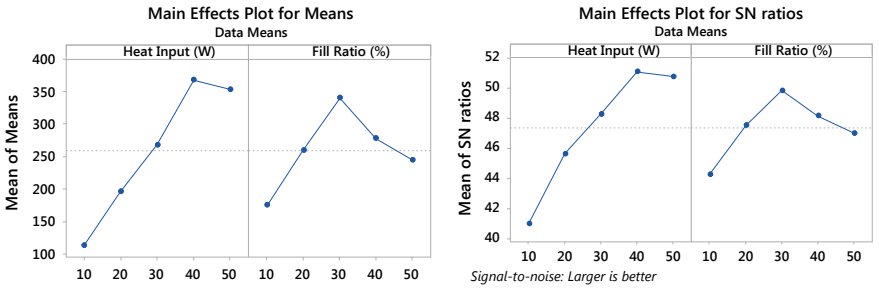

Fig. 16 Effect on heat transfer coefficient

Table 11 Response table for heat transfer coefficient

Level	Heat input (W)	Fill ratio (%)
1	40.99	44.26
2	45.63	47.52
3	48.28	49.84
4	51.10	48.16
5	50.78	47.00
Delta	10.10	5.58
Rank	1	2

5.2 Analysis of Variance

See Table 12.

The ANOVA table for thermal resistance shows that the contribution of heat input is 81.31%, and the contribution of fill ratio is 15.97%.

The ANOVA table for heat transfer coefficient shows that the contribution of heat input is 72.83% and the fill ratio is 22.38% (Table 13).

Table 12 ANOVA for thermal resistance

Source	DF	Seq SS	Contribution (%)	Adj SS	Adj MS	*F*-value	*P*-value
Heat input (W)	4	1.53474	81.31	1.53474	0.383684	119.75	0.000
Fill ratio (%)	4	0.30147	15.97	0.30147	0.075367	23.52	0.000
Error	16	0.05126	2.72	0.05126	0.003204		
Total	24	1.88747	100.00				

Table 13 ANOVA for heat transfer coefficient

Source	DF	Seq SS	Contribution (%)	Adj SS	Adj MS	*F*-value	*P*-value
Heat input (W)	4	229,054	72.83	229,054	572,63.5	60.79	0.000
Fill ratio (%)	4	70,386	22.38	70,386	175,96.5	18.68	0.000
Error	16	15,071	4.79	15,071	941.9		
Total	24	314,511	100.00				

6 Conclusion

Theoretical thermal design calculations were performed in the heat pipes with R134a and R404a as working fluid. It was found that the maximum heat transfer limit of the heat pipe with R134a is 118.9 W and R404a is 158.9 W. Temperature distribution plots for both heat pipes were obtained and are validated with the experimental values. The thermal resistance for the heat pipe using R134A as the working fluid is 0.35 K/W and R404a as the working fluid is 0.225 K/W. The average relative error in the thermal resistance is found to be 6.115%. The thermal resistance value is low for 30% fill ratio. Employing this type of heat pipes results in less thermal resistance. Optimization was done using Taguchi technique.

References

1. Gorecki G (2018) Investigation of two-phase thermosyphon performance filled with modern HFC refrigerants. Heat Mass Transf 2018(54):2131–2143
2. Haghshenasfard M, Asmaie A, Mehrabani-Zeinabad A, Nasr Eshahany M (2013) Thermal performance analysis of nanofluids in a thermosyphon heat pipe using CFD modeling. Springer. http://dx.doi.org/10.1007/s00231-013-1110-6
3. Rahimi M, Alizadehdakhel A, Alsairafi AA (2009) CFD modeling of flow and heat transfer in a thermosyphon. Int Commun Heat Mass Transf
4. Sozen A, Menlik T, Guru M, Irmark AF, Kilic F, Akta M (2014) Utilization of fly ash nanofluids in two-phase closed thermosyphon for enhancing heat transfer. Exp Heat Transf

5. Vafai K, Shafahi M, Bianco V, Manca O (2010) Thermal performance of flat-shaped heat pipes using nanofluids. Int J Heat Mass Transf
6. Khandekar S, Battacharya B, Paralikar S, Jaipurkar T (2017) Thermo-mechanical design and characterization of flexible heat pipes. Appl Therm Eng. http://dx.doi.org/10.1016/j.applthermaleng.2017.01.036
7. Jouhara H, Merchant H (2011) Experimental investigation of a thermosyphon based heat exchanger used in energy efficient air handling units. Energy. http://dx.doi.org/10.1016/j.energy.2011.08.054
8. Senthilkumar R, Vaidyanathan S, Sivaraman B (2010) Thermal analysis of heat pipe using Taguchi method. Int J Eng Sci Technol 2(4):564–569
9. Narayan A, Jaipurkar T, Khandekar S, Paralikar S (2015) Development and testing of flexible heat pipes. In: Proceedings of the 23rd national heat and mass transfer conference and 1st international ISHMT-ASTFE heat and mass transfer conference
10. Panda KK, Basak A, Dulera IV (2015) Design and development of high temperature heat pipes and thermosiphons for passive heat removal from compact high temperature reactor. In: Thorium energy conference
11. Huminic G, Huminic A (2009) CFD study of the heat pipes with water-nanoparticles mixture. In: Fourth European automotive simulation conference
12. Deshpande A, Patil V, Patil R (2016) Theoretical design of radiator using heat pipes. Int J Eng Res Technol 5(11)
13. Wrobel LC, Jouhara H, Fadhl B (2015) CFD modelling of a two-phase closed thermosyphon charged with R134a and R404a. Appl Therm Eng
14. El-Sharkawy A, Uddin A (2016) Evaluation of heat pipe heat exchanger for automotive applications. SAE Int
15. Umberto Costa Bitencourt J (2016) CFD simulation of a Pulsating heat pipe using ANSYS Fluent. Res Gate
16. Bhanu Prakash S, Raghuram J, Phani Kumar KVNK, Khiran GV, Snehith K (2017) Thermal Performance of a selected heat pipe at different tilt angles. IOP Conf Ser: Mater Sci Eng
17. Girish S, Lavanya K, Geeta Krishna P (2017) CFD analysis of Pulsating heat pipe using different fluids. Int J Mech Eng Technol
18. Pandiraj P, Gnanavelbabu A, Saravanan P (2018) Experimental and statistical analysis of MgO nanofluids for thermal enhancement in a novel flat plate heat pipes. Int J Nanosci